UNIVERSITY *of York*

This is a repository copy of *Novel mesoporous carbon-silica composites from vinasse for the removal of dyes from aqueous silk dyeing wastes*.

White Rose Research Online URL for this paper:
https://eprints.whiterose.ac.uk/192044/

Version: Published Version

Article:

White Rose
university consortium
Universities of Leeds, Sheffield & York

eprints@whiterose.ac.uk
https://eprints.whiterose.ac.uk/

Novel mesoporous carbon-silica composites from vinasse for the removal of dyes from aqueous silk dyeing wastes

Tippawan Ponnikorn[1], Jesper T. N. Knijnenburg[2], Duncan J. Macquarrie[3] and Yuvarat Ngernyen*[1]

[1]Biomass & Bioenergy Research Laboratory, Department of Chemical Engineering, Faculty of Engineering, Khon Kaen University, Khon Kaen 40002, Thailand
[2]Biodiversity and Environmental Management Division, International College, Khon Kaen University, Khon Kaen 40002, Thailand
[3]Green Chemistry Centre of Excellence, Department of Chemistry, University of York, YO10 5DD, UK

Abstract

Novel mesoporous carbon-silica composites were prepared from vinasse, a by-product from ethanol production, as the carbon source, and sodium silicate (Na_2SiO_3) and potassium silicate (K_2SiO_3) as low-cost silica source alternatives to tetraethyl orthosilicate (TEOS). The composites were characterized for their surface area and porous properties using nitrogen adsorption-desorption porosimetry. The composites possessed a high mesopore volume (45-77%) with moderate specific surface areas (343-656 m^2/g) and pore size of 3.12-5.58 nm. The adsorption behaviour of carbon-silica composites for the removal of four silk dyes (Green 41, Blue 32, Dark red 34 and Dark gold brown 35) from aqueous solution was investigated and compared with a commercial activated carbon. The effects of adsorption time, dye concentration, pH and temperature were analyzed. The dye adsorption kinetics of all four dyes followed the pseudo-second order kinetic model, suggesting chemisorption as the dominant mechanism. Moreover, the intraparticle diffusion model showed that both internal diffusion and external diffusion were rate-limiting. The maximum adsorption capacities for all dyes were found at pH ~ 2. The equilibrium data for silk dyes adsorption were best described by the Langmuir equation, thus indicating monolayer adsorption. Thermodynamic parameters indicated that the dye adsorption was an endothermic process ($\Delta H > 0$). The negative values of free energy (ΔG) confirmed that dye adsorption was spontaneous at the investigated temperatures (303-323 K). For all dyes, the maximum adsorption capacities of carbon-silica composites were comparable to the commercial activated carbon. The combination of vinasse with low-cost silica sources is a promising approach to produce inexpensive carbon-silica composites for application as adsorbents for dye removal from aqueous waste solutions generated during silk manufacture and dyeing.

Keywords: Vinasse, Mesoporous, Carbon-silica composite, Adsorbent, Silk dye

1. Introduction

Khon Kaen province is one of Thailand's most famous silk regions. Silk processing from cocoons to the clothing has many steps include reeling, weaving, degumming, dyeing and finishing [1]. Since silk fiber has a slightly cationic character, dyes such as acid dyes, metal complex dyes, and reactive dyes are used, of which acid dyes are most suitable for silk [1]. The effluent left from the silk dyeing process exhibits an intense color and causes serious environmental problems. Different methods are applied to remove acid dyes such as coagulation/flocculation [2], electrocoagulation [3] or a hybrid treatment system (biological and ozonation) [4]. Adsorption by porous materials is one of the most promising methods for dye removal due to the simplicity of the process and lower cost involved compared to other processes. Adsorption of various textile dyes has been examined, most commonly with commercial acid dyes such as Congo red [4], acid red 398 [2] or acid violet 17 [5]. However, there is only a limited number of studies that use domestic real dyes. Therefore, this study focused on developing a process for removing real silk dyes from aqueous solutions.

Activated carbon is a widely used adsorbent but the price of commercial activated carbon produced from coal or wood is very high, which limits its applications. Thus, an industrial by-product could be considered for utilization as an adsorbent. Vinasse is a by-product of the ethanol production from molasses. It is rich in organic matter and minerals, has a dark brown color and unpleasant odor, and is often used as fertilizer. However, vinasse has an extensive environmental impact because it increases Chemical Oxygen Demands (COD) levels in groundwater reservoirs and vinasse-derived ions leach into water bodies when used as fertilizer coupled with irrigation in sugarcane fields [6]. Therefore, this work attempted to find an alternative use for vinasse.

The design of new composite materials that combine and improve the properties of individual components is a growing research area of interest. In the past several decades, mesoporous carbon-silica composites (CSCs) have been developed for use in many important applications such as catalyst supports [7], reinforcing materials [8], energy storage [9] and adsorbents [10]. In many processes, CSCs exhibit superior properties to their separate components, as a result of a combination between the properties of meso-ordered silica that are elevated surface area and ordering in a wide range of pore structure and the properties of carbons that are electrical conductivity, thermal stability, and easy to modify its surface chemistry [11].

Examples of carbon sources to prepare CSCs are activated carbon [12-14], polyfurfuryl alcohol [15], pyrolysis of CH_2Cl_2 [15] and novolac-type phenol-formaldehyde resin [16]. As silica source, tetraethyl orthosilicate (TEOS) [12, 14], water glass ($SiO_2:Na_2O$ = 3.35) [13], MCM-41/TMAOH/TMASi [15], silica gel [15, 16] and pyrogenic silica A-300 [17] are commonly used. To the best of our knowledge there is no report describing the preparation of CSC from vinasse. According to Noa-Bolaño et al. [18] the composition of vinasse by weight was 93% water, 1.46% glycerol ($C_3H_8O_3$), 1.27% fumaric acid ($C_4H_4O_4$), 1.21% lactic acid ($C_3H_6O_3$), 0.91% ethanol (C_2H_5OH), 0.83% sucrose ($C_{12}H_{22}O_{11}$), 0.76% L-glutamic acid ($C_5H_9NO_4$), 0.33% potassium oxide (K_2O), 0.11% sodium sulfate (Na_2SO_4), 0.05% magnesium oxide (MgO), 0.05% calcium oxide (CaO) 0.049% and 0.002% diphosphorus pentaoxide (P_2O_5). Vinasse thus contains various carbon-containing compounds and can be use as carbon source to prepare CSC. Moreover, the most commonly used silica sources such as TEOS are not available in Thailand and need to be imported from abroad, which greatly increases their cost. In order to develop a more cost-effective synthesis route, we aimed to use low-cost and locally available silica sources that are Na_2SiO_3 and K_2SiO_3, which are approximately 100 times cheaper than TEOS. Several recent studies have prepared CSCs via impregnation of carbon and silica sources followed by carbonization at high temperature of 300-800°C under inert atmosphere [15-17, 19]. To avoid this complicated method and energy cost, our novel work used a single step process at low temperature.

The purpose of this work was to synthesize novel CSCs by using vinasse as carbon source and Na_2SiO_3, K_2SiO_3 and TEOS as silica sources, and to characterize the materials to understand the nature of the resulting nanoporosity. Synthesis conditions with varying chemical ratios between vinasse and silica source were investigated in relation to material surface area by N_2 adsorption. The performance in domestic real silk dye adsorption was investigated in a batch mode. The effects of variables such as contact time, initial dye concentration, pH and temperature were investigated. Kinetics, equilibrium adsorption isotherms and thermodynamics were also evaluated. The kinetic data were analyzed using the pseudo-first order and the pseudo-second-order models and the adsorption isotherms were modeled with the Langmuir and Freundlich isotherms. A commercially available activated carbon (CAC) was studied for comparison.

2. Materials and methods

2.1 Chemicals

Vinasse was collected from Mitr Phol Biofuel Company Limited (Phu Khiao). This company used molasses from sugar production of sugar cane as starting material. Na_2SiO_3 and K_2SiO_3 solutions were acquired from C. Thai Chemicals. TEOS solution was purchased from Sigma-Aldrich, Germany. Sulfuric acid (H_2SO_4) was obtained from ANaPURE, New Zealand. Commercial activated carbon was supplied by C. Gigantic Carbon Co.,Ltd.

2.2 Synthesis and characterization of Carbon-Silica Composite (CSC)

The novel CSCs were synthesized by mixing various amounts of vinasse with 20 mL of 50% H_2SO_4 and 5 mL of distilled water to create the carbon source. Then, 5 g of silica source (Na_2SiO_3, K_2SiO_3 or TEOS) was added to the carbon source with weight ratio of vinasse to silica source ranging from 1:1 to 20:1. During this stage a liquid gel was formed, which was magnetically stirred at 500 rpm at 85°C for 6 h. The sample was rinsed several times with water until the pH of the washed water was equal to the starting water. Finally, the wet sample was dried at 130°C for 6 h in an oven. A blank experiment was also conducted without silica source but keeping other parameters the same as those for the CSCs.

The synthesized CSCs were characterized for their specific surface area, pore volume and average pore size by N_2 adsorption at 77 K using ASAP 2460 (Micromeritics). Before the test, the samples were evacuated at 150°C under vacuum. The specific surface area of the sample was calculated by the Brunauer-Emmett-Teller (BET) equation based on the adsorption data at a relative pressure range P/P^o of 0.05-0.3. The micropore volume was analyzed using Dubinin-Radushkevich (DR) method. The total pore volume was obtained using the adsorbed amount of N_2 at $P/P^o = 0.99$, and the mesopore volume was determined by subtracting the micropore volume from the total pore volume. The average pore size was calculated according to the Barrett-Joyner-Halenda (BJH) model. Vinasse and composite samples were characterized by FTIR spectroscopy in ATR mode with the wavenumber ranging of 500-4000 cm^{-1} and 32 scans by using ALPHA II (Bruker). Thermal stability of the composites was characterized by using DTG-60H (Shimadzu) under air atmosphere with a constant heating rate of 10°C/min over the temperature range of 25 to 950°C.

2.3 Batch adsorption study of silk dye

The silk dyes used in this study were brands and colors that are commonly used in household silk making in Chonnabot district, Khon Kaen province. Therefore, four colors (Green 41, Dark gold brown 35, Blue 32 and Dark red 34) with the brand name Lion Drumming were selected as adsorbates. Dye adsorption experiments were carried out in batch mode using 0.01 g of adsorbent and 50 mL of dye solution. After adsorption, the sample was centrifuged at 3500 rpm for 30 min and the dye concentration was determined using UV-VIS Spectrophotometer (Analytik Jena). The maximum wavelengths of detection were 392, 395, 635 and 523 nm for Green 41, Dark gold brown 35, Blue 32 and Dark red 34, respectively. To study the effect of contact time on dye adsorption, each adsorbent was added to 100 mg/L dye solution for different time intervals between 5-720 min at room temperature and given pH. The dye solution with initial concentration of 100 mg/L was adjusted pH to 2-10 by using 0.1 M HCl or NaOH to study the effect of solution pH on the adsorption process. To study the effect of initial dye concentration, dye solutions with concentrations between 50-1000 mg/L were prepared and adsorption experiments were conducted at room temperature and optimum pH. Finally, the effect of temperature was studied at 303, 313 and 323 K by using 100 mg/L dye solution and optimum pH. The amount of dye adsorbed, q (mg/g) was calculated by the expression

$$q = \frac{(C_o - C)V}{W} \tag{1}$$

where C_o and C are the initial and at time t dye solution concentrations (mg/L), respectively, V is the volume of dye solution (L) and W is the weight of adsorbent used (g).

3. Results and discussion

3.1 Characteristics of the obtained carbon-silica composites

The surface areas of the CSCs prepared at various carbon to silica source ratios are shown in Table 1. The carbon to silica source ratio played an important role on the surface area of resulting composites. Using only vinasse (i.e., only carbon source without silica) did not result in a porous material as evidenced by the low specific surface area of 1.98 m^2/g. Upon addition of silica source, the surface area increased with increasing this ratio from 1 to 2 for Na_2SiO_3 and K_2SiO_3 and 1 to 5 for TEOS. However, further increasing the ratio caused a decrease in surface area. The maximum surface areas were obtained as 375, 343 and 656 m^2/g for using Na_2SiO_3, K_2SiO_3 and TEOS as silica source, respectively. This indicated that low-cost and locally available silica sources (Na_2SiO_3 and K_2SiO_3) could produce porous materials with surface areas comparable to more expensive TEOS. The composites prepared at these optimum ratios were chosen as adsorbent for real silk dyes adsorption. These optimum CSCs prepared with Na_2SiO_3, K_2SiO_3 and TEOS are named CSC-Na, CSC-K, and CSC-T, respectively.

Table 1 Surface area of the obtained CSCs at various carbon to silica source ratio

Vinasse: silica weight ratio	Surface area (m^2/g)		
	Na_2SiO_3	K_2SiO_3	TEOS
Only vinasse, no silica source		1.98	
1:1	368	289	399
2:1	375*	343*	418
3:1	368	310	469
4:1	366	268	494
5:1	250	266	656*
10:1	241	266	420
15:1	201	209	377
20:1	188	172	245

* Highest surface area

The N_2 adsorption-desorption isotherms of the composites prepared at the optimum ratio and commercial activated carbon (CAC) are shown in Figure 1. Isotherms of CSC-Na and CAC were classified as a mixture of Type I and Type IV, while that of CSC-K and CSC-T were of Type IV. According to International Union of Pure and Applied Chemistry or IUPAC classification, Type I isotherm can be associated with micropore structure while Type IV isotherm exhibited the mesoporous material. The pore structure parameters of the obtained CSCs and CAC were calculated according to the isotherms are listed in Table 2. Both CSC-K and CSC-T contained mainly mesopore volume (over 70%) and had a mean pore size of ~ 5 nm. CSC-Na contained comparable micropore and mesopore volume and had a smaller mean pore size of CSC-Na of 3.12 nm. The CAC had the highest surface area of 1130 m^2/g with mainly mesopore volume (96%) but mean pore size around 3 nm. Therefore, the adsorbents for real silk dyes adsorption can be divided into three types: (1) CSCs prepared from K_2SiO_3 and TEOS represented a moderate surface area with mainly mesopores and larger mean pore size, (2) CSC prepared from Na_2SiO_3 represented a moderate surface area with both micropores and mesopores and a smaller pore size and (3) CAC represented a high surface area with mainly mesopores but smaller mean pore size.
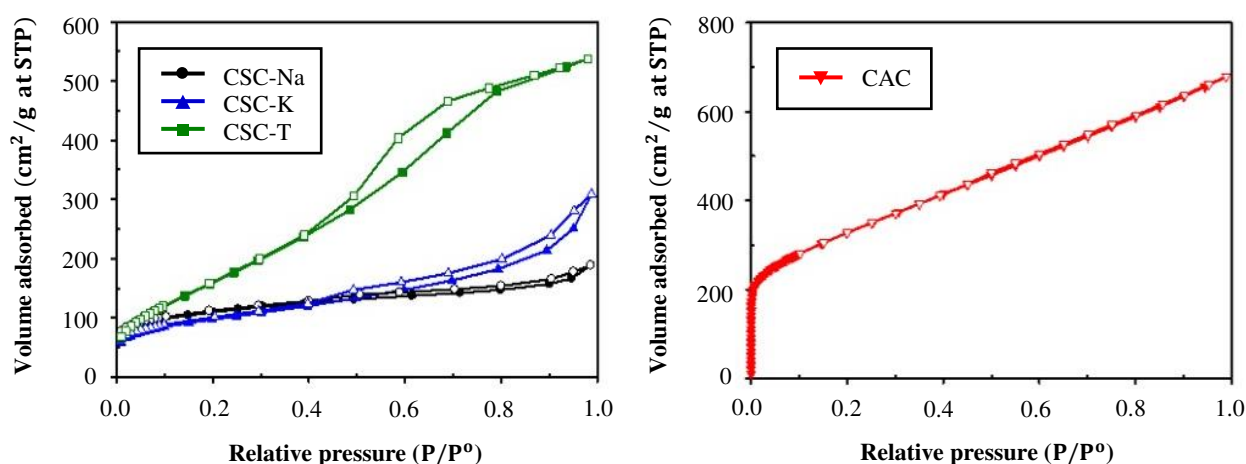
Figure 1 N_2 Isotherms of CSCs prepared at optimum ratio and commercial activated carbon (CAC)

Table 2 Textural properties of CSCs prepared at optimum ratio and CAC

Adsorbent	Surface area (m^2/g)	Micropore volume (cm^3/g)	Mesopore volume (cm^3/g)	Total pore volume (cm^3/g)	Mean pore size (nm)
CSC-Na	375	0.16 (55%)	0.13 (45%)	0.29	3.12
CSC-K	343	0.14 (29%)	0.34 (71%)	0.48	5.58
CSC-T	656	0.19 (23%)	0.64 (77%)	0.83	5.06
CAC	1130	0.05 (4%)	1.00 (96%)	1.05	3.72

Figure 2 shows the compared FTIR spectra of vinasse and CSCs. The broad band at 3340 cm^{-1} and the strong peak at 1634 cm^{-1} in vinasse were assigned to O-H stretching vibrations in alcohol and possibly some water in sample [14, 20]. These results are in agreement with the composition of vinasse, which contains mainly water and various small organic molecules such as ethanol and lactic acid [18]. Both bands significantly decreased for all composites. Similar absorption bands were observed in all composite samples. The peaks at 797 and 1060 cm^{-1} were assigned to Si-O and Si-O-Si vibrations [21] and the peak at 950 cm^{-1} was ascribed to Si-OH [22].
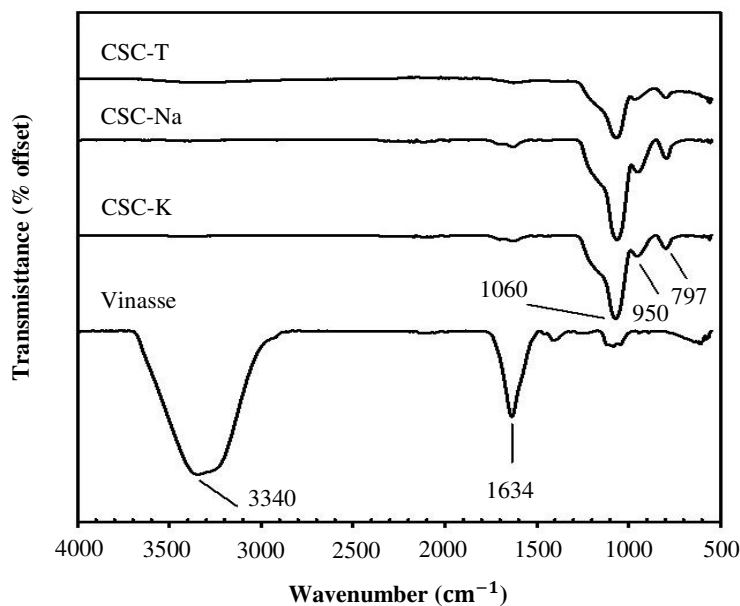

Figure 2 FTIR Spectra of vinasse and CSCs prepared at optimum ratio

Thermal stability analysis of composites using TGA is shown in Figure 3. The composites had a high thermal stability, since the total weight loss after oxidation was 33-38%. This may be due to the high thermal stability of silica. The weight loss between 300°C to 500°C was due to the combustion of carbon, and the weight remained constant above 500°C. The final residue of 62-67% was ash.
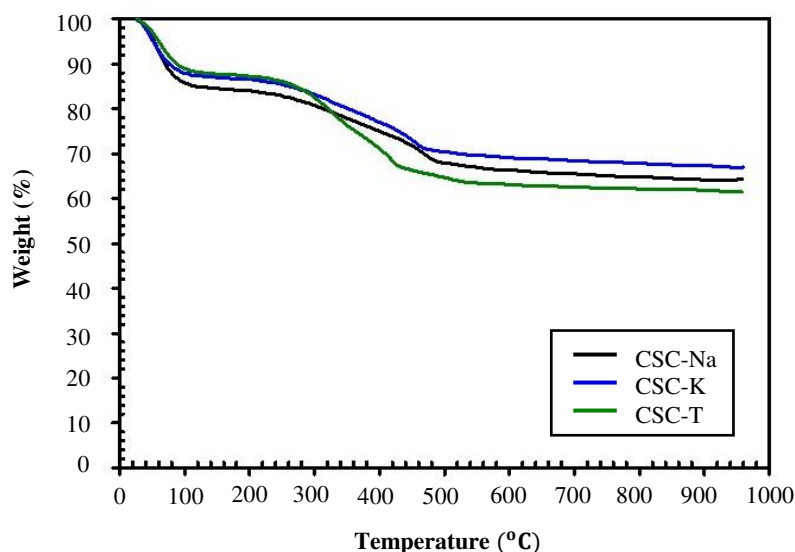

Figure 3 TGA Results in air atmosphere of CSCs prepared at optimum ratio

In addition to the most important application of carbon-silica composite as adsorbent, other applications include the use as insulator material, lithium-ion battery anode material or biosensors [23]. Therefore, these composites should be characterized for their thermal conductivity, compressive strength, energy density, charge/discharge process, sensitivity and chemical stability in future for more advantage. However, the main disadvantage of composites is high ash content (from TGA results). In addition, the using of ash remained from composite should be study in future.

3.2 Effect of contact time on silk dye adsorption

The dye adsorption kinetics were studied up to 720 min for a fixed amount of adsorbent (0.01 g) at an initial dye concentration of 100 mg/L. As can be seen in Figure 4, the dye molecules rapidly adsorbed onto the adsorbents' surface at the beginning of the adsorption process. As time passed, the adsorption process slowed down until equilibrium was established. The time to reach equilibrium and the amount adsorbed at equilibrium for each dye are summarized in Table 3. All CSCs had the same equilibrium time for each dye, namely

150, 250, 200 and 400 min for Green 41, Blue 32, Dark red 34 and Dark gold brown 35, respectively. Moreover, the CSC samples reached equilibrium faster than CAC, which can be attributed to the more favorable porous structures of CSCs, i.e. the interior sites were more easily accessible. For all dyes, the amount adsorbed onto the CSCs followed the order CSC-T > CSC-K > CSC-Na. However, CAC had higher adsorbed amount than CSCs except in the case of Dark red 34. This may be due to the higher surface area and pore volume of CAC than CSCs. When compared with CAC, the application of CSC samples had an advantage of a shorter equilibrium time.
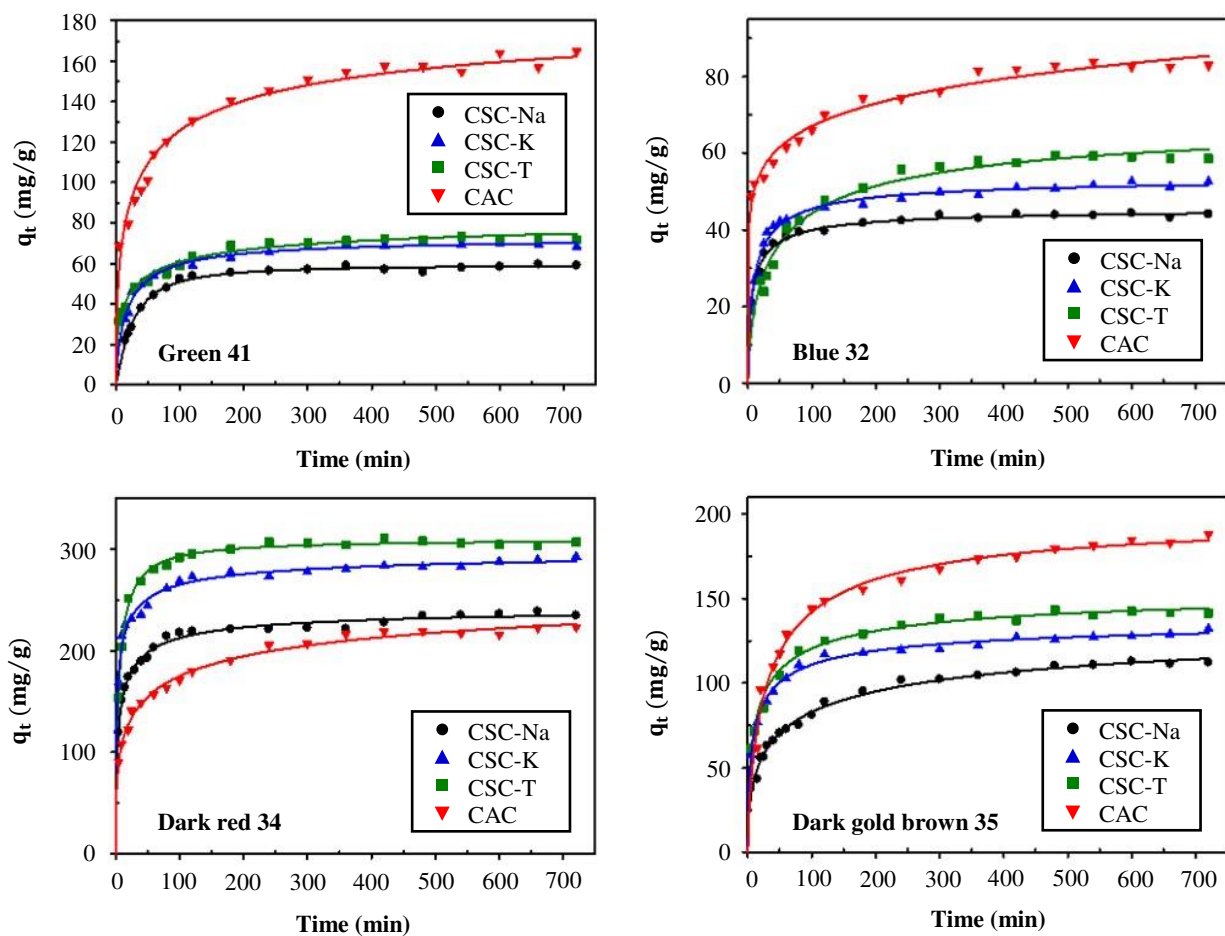
Figure 4 Effect of contact time on adsorption of real silk dyes (C_o = 100 mg/L; pH = 6.5 for Green 41 and Dark gold brown 35, 6.2 for Blue 32, 6.4 for Dark red 34; amount of adsorbent 0.01 g/50 mL; room temperature)

Table 3 Equilibrium time and amount adsorbed at equilibrium for each real silk dye

Adsorbent	Equilibrium time (min)	Amount adsorbed at equilibrium (mg/g)
Green 41		
CSC-Na	150	59.52
CSC-K	150	69.73
CSC-T	150	73.22
CAC	400	164.84
Blue 32		
CSC-Na	250	44.39
CSC-K	250	52.63
CSC-T	250	59.45
CAC	400	83.82
Dark red 34		
CSC-Na	200	238.82
CSC-K	200	292.80
CSC-T	200	311.25
CAC	400	223.36
Dark gold brown 35		
CSC-Na	400	112.90
CSC-K	400	132.18
CSC-T	400	143.26
CAC	500	187.97

3.3 Kinetic studies

Kinetic studies for adsorption process provide information about the relationship between adsorbent and adsorbate in terms of adsorption rate and rate-limiting step, and can provide information on the mechanisms involved during the adsorption process. The adsorption rate is an important factor for adsorbent selection. The adsorbent should have a large adsorption capacity and a fast adsorption rate [24]. In this study, two common kinetic models (pseudo-first order and pseudo-second order) were used to describe the dye adsorption onto CSCs and CAC [25]:

$$\log(q_e - q_t) = \log q_e - \frac{k_1 t}{2.303} \tag{2}$$

$$\frac{t}{q_t} = \frac{1}{k_2 q_e^2} + \frac{t}{q_e} \tag{3}$$

Here, q_e is amount adsorbed at equilibrium time (mg/g), q_t is amount adsorbed (mg/g) at time t (min), k_1 and k_2 are the pseudo-first order (1/min) and pseudo-second order (g/mg·min) rate constants, respectively. The kinetic rate constant and q_e for each model can be calculated by plotting log (q_e-q_t) versus t for pseudo-first order and t/q_t versus t for pseudo-second order model, and the graphs are presented in Figure 5. The kinetic parameters for both kinetic models were calculated from the graph and are presented in Table 4. The higher k_1 values of CSCs indicated that the rate of dye removal was faster than CAC except in the case of Dark red 34. The CSCs also exhibited higher values of k_2 than CAC except in the case of Blue 32. This clearly shows that the adsorption rate onto CSCs was faster than CAC. This means that the CSC samples show a considerable higher rate of real silk dye removal than CAC.

The correlation coefficients (R^2) for the pseudo-second order model were greater than pseudo-first order model and closer to unity, which implied that the experimental data were in good agreement with the pseudo-second order model. Furthermore, the q_e values calculated based on the pseudo-second order model were very close to the experimental values (Table 3). Therefore, it can be concluded that the adsorption of real silk dyes onto CSCs and CAC were controlled by chemisorption.
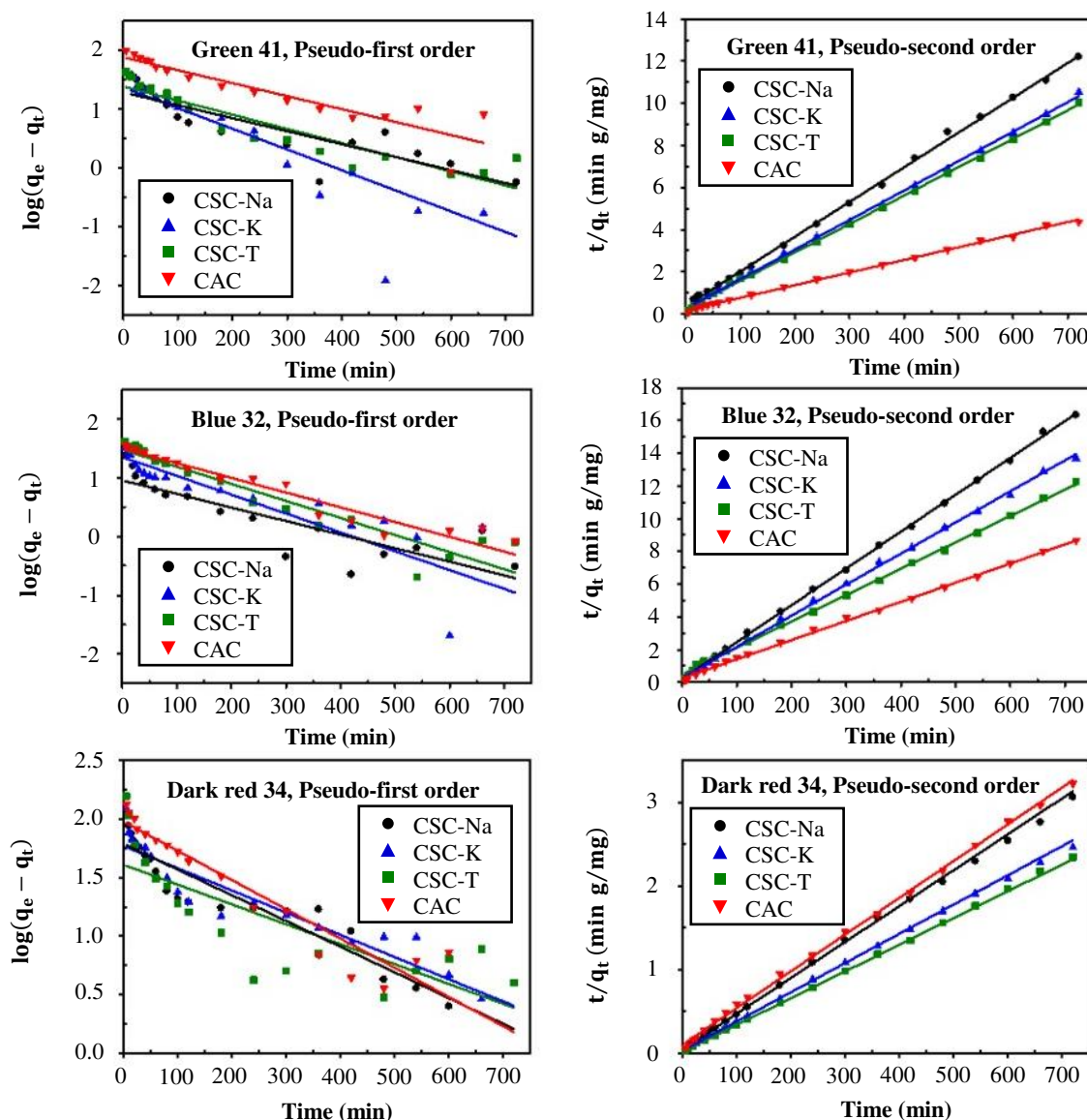

Figure 5 Fitting of pseudo-first order and pseudo-second order kinetic models of real silk dyes
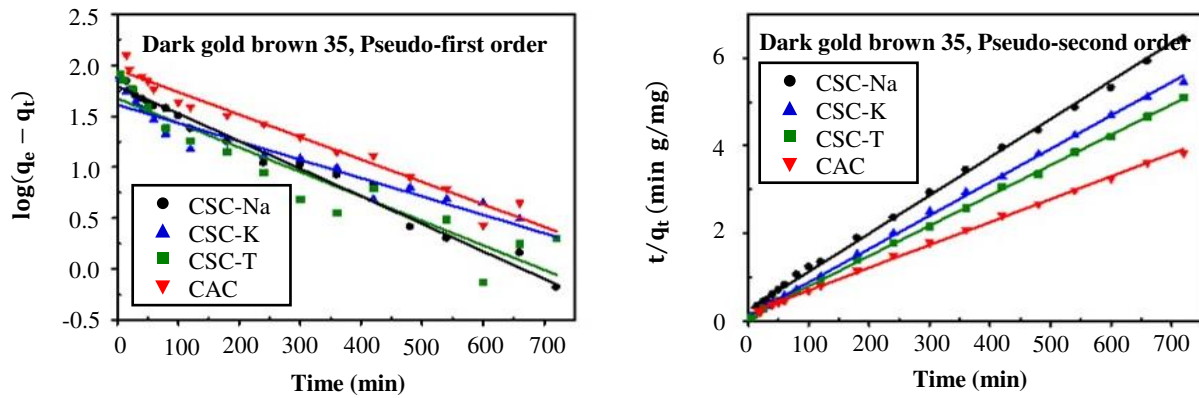
Figure 5 (Continued) Fitting of pseudo-first order and pseudo-second order kinetic models of real silk dyes

Table 4 Kinetic parameters of real silk dyes on CSCs and CAC

Kinetic models	Parameters	Adsorbent			
		CSC-Na	CSC-K	CSC-T	CAC
		Green 41			
Pseudo-first order	$q_{e,cal}$ (mg/g)	19.11	23.00	24.02	75.13
	k_1 (1/min)	5.067×10^{-3}	8.060×10^{-3}	5.527×10^{-3}	5.067×10^{-3}
	R^2	0.765	0.691	0.861	0.831
Pseudo-second order	$q_{e,cal}$ (mg/g)	60.61	71.43	74.07	166.67
	k_2 (g/mg·min)	7.407×10^{-4}	7.501×10^{-4}	8.104×10^{-4}	2.168×10^{-4}
	R^2	0.999	0.999	0.999	0.998
		Blue 32			
Pseudo-first order	$q_{e,cal}$ (mg/g)	8.890	22.21	29.61	31.06
	k_1 (1/min)	5.297×10^{-3}	7.370×10^{-3}	6.679×10^{-3}	5.758×10^{-3}
	R^2	0.735	0.793	0.892	0.934
Pseudo-second order	$q_{e,cal}$ (mg/g)	44.44	52.63	62.11	85.47
	k_2 (g/mg·min)	2.393×10^{-3}	1.338×10^{-3}	5.141×10^{-4}	5.706×10^{-4}
	R^2	0.999	0.999	0.999	0.999
		Dark red 34			
Pseudo-first order	$q_{e,cal}$ (mg/g)	61.55	58.94	40.78	95.28
	k_1 (1/min)	5.067×10^{-3}	4.376×10^{-3}	3.915×10^{-3}	5.758×10^{-3}
	R^2	0.852	0.878	0.639	0.908
Pseudo-second order	$q_{e,cal}$ (mg/g)	232.56	285.71	312.50	227.27
	k_2 (g/mg·min)	4.878×10^{-4}	4.640×10^{-4}	6.649×10^{-4}	1.990×10^{-4}
	R^2	0.999	0.999	0.999	0.999
		Dark gold brown 35			
Pseudo-first order	$q_{e,cal}$ (mg/g)	62.44	41.05	47.14	90.28
	k_1 (1/min)	6.218×10^{-3}	4.145×10^{-3}	5.527×10^{-3}	5.067×10^{-3}
	R^2	0.977	0.908	0.888	0.965
Pseudo-second order	$q_{e,cal}$ (mg/g)	114.94	131.58	144.93	192.31
	k_2 (g/mg·min)	2.932×10^{-4}	4.477×10^{-4}	4.429×10^{-4}	1.497×10^{-4}
	R^2	0.998	0.999	0.999	0.999

In order to further clarify the rate-limiting step, the adsorption process of real silk dyes onto CSCs and CAC samples was analyzed by the intraparticle diffusion model, expressed as follows [26]:

$$q_t = k_p t^{1/2} + I \tag{4}$$

where k_p (mg/g·min$^{1/2}$) and I (mg/g) are the intraparticle diffusion rate constant and intercept of the linear plot of q_t against $t^{1/2}$ which is proportional to the thickness of the boundary layer and can be used to judge whether intraparticle diffusion is the only rate-limiting step or not [27]. According to this model, the adsorption process involves 3 steps: (1) the adsorbate moves through the boundary layer via film diffusion onto the external adsorbent surface, (2) the adsorbate moves from the external surface into interior pores via pore diffusion or intraparticle diffusion (which is the rate-limiting step), and (3) the adsorbate is adsorbed onto the active sites at the interior porous surface until the final equilibrium step is reached [27, 28].

As shown in Figure 6, the linear plots of intraparticle diffusion model showed two stages of adsorption, and the lines did not pass through the origin. These indicated that the adsorption of silk dyes on CSCs and CAC was dominated by the combined effect of adsorption by surface adsorption (stage 1) and then followed by the intraparticle diffusion process (stage 2). Thus, the intraparticle diffusion was not the only rate-limiting step. The corresponding fitting parameters and the correlation coefficients (R^2) were determined by linear regression and are listed in Table 5. The larger k_p values suggest a larger intraparticle diffusion rate [27]. The I value of all samples increased from the first stage, which indicated that the boundary layer had a significant influence on the adsorption of silk dyes on CSCs and CAC. At the second stage, the active sites were exhausted and the diffusion became more difficult, resulting in much lower k_p values than the first stage.
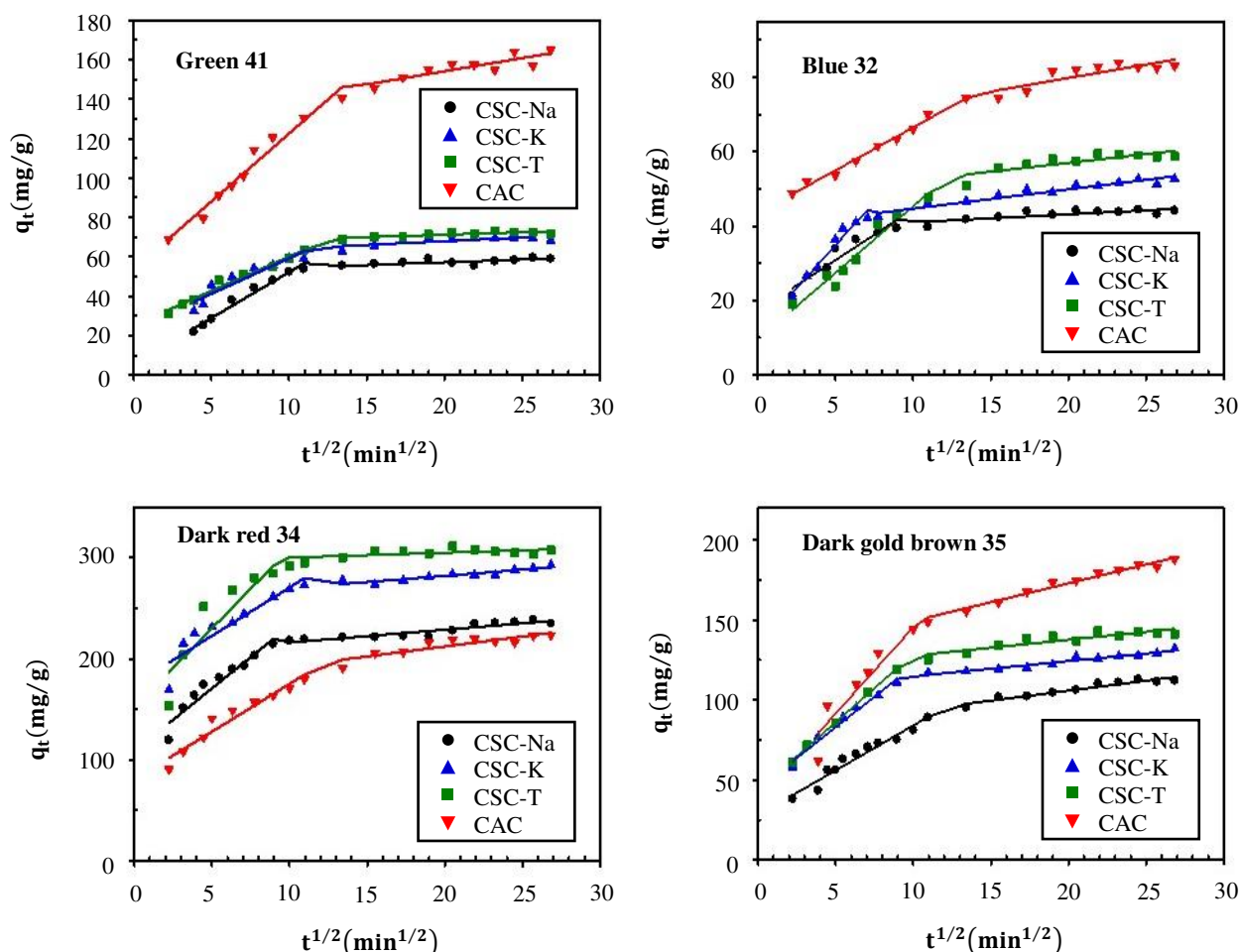
Figure 6 Linear plots of intraparticle model for real silk dyes adsorption on CSCs and CAC

Table 5 Intraparticle diffusion model constants for real silk dyes adsorbed on CSCs and CAC

Stage	Parameters	Adsorbent			
		CSC-Na	CSC-K	CSC-T	CAC
		Green 41			
1	k_P (mg/g·min$^{1/2}$)	4.658	3.608	3.476	6.896
	I (mg/g)	5.617	23.185	25.287	53.590
	R^2	0.974	0.875	0.976	0.969
2	k_P (mg/g·min$^{1/2}$)	0.276	0.379	0.254	1.336
	I (mg/g)	51.669	60.352	66.128	127.440
	R^2	0.646	0.558	0.723	0.739
		Blue 32			
1	k_P (mg/g·min$^{1/2}$)	2.725	4.627	3.580	2.305
	I (mg/g)	17.214	11.674	9.488	43.416
	R^2	0.903	0.961	0.956	0.990
2	k_P (mg/g·min$^{1/2}$)	0.215	0.516	0.474	0.723
	I (mg/g)	38.848	39.516	47.487	65.314
	R^2	0.637	0.928	0.682	0.684
		Dark red 34			
1	k_P (mg/g·min$^{1/2}$)	12.411	9.574	15.676	9.453
	I (mg/g)	108.820	174.920	151.84	80.773
	R^2	0.923	0.860	0.828	0.941
2	k_P (mg/g·min$^{1/2}$)	1.261	1.230	0.474	1.975
	I (mg/g)	203.650	257.550	295.520	172.770
	R^2	0.867	0.856	0.331	0.782
		Dark gold brown 35			
1	k_P (mg/g·min$^{1/2}$)	5.613	7.644	8.525	10.791
	I (mg/g)	27.915	44.708	43.450	37.498
	R^2	0.955	0.980	0.998	0.896
2	k_P (mg/g·min$^{1/2}$)	1.245	0.945	0.997	2.357
	I (mg/g)	80.823	105.350	117.690	125.79
	R^2	0.924	0.938	0.796	0.967

3.4 Effect of initial pH on silk dye adsorption

The solution pH is a significant parameter affecting dye adsorption onto adsorbent. This experiment was performed at room temperature with 0.01 g adsorbent and 50 mL of dye solution. The initial dye concentration was 100 mg/L by varying the pH from 2 to 12 and the sample was equilibrated at time as shown in Table 3. Figure 7 shows that the adsorption of real silk dyes onto CSCs and CAC was strongly dependent on the initial solution pH. Dye adsorption was higher at low pH and decreased with increasing pH value from 2 to 12, except in the case of Dark red 34 by CAC. This means that the anionic dye molecules were easily adsorbed in acidic conditions. At higher pH, the amount adsorbed decreased because the surface of the adsorbent was more protonated and competitive adsorption occurred between H^+ and free dye ions and their OH^- towards the adsorption sites [29]. Similar pH-dependent adsorption behavior of acid dyes was observed for acid red 1 (AR1) on cellulose-g-p (AA-co-AM) bio-adsorbent [30], acid red 88 (AR88) on *Azolla filiculoides* [29] and *Lemna minor* [31] and Congo red on sawdust [32]. Based on the adsorption capacities, the optimum pH of 2 was selected for all further experiments, except in the case of Dark red 34 adsorption by CAC which used pH 8.
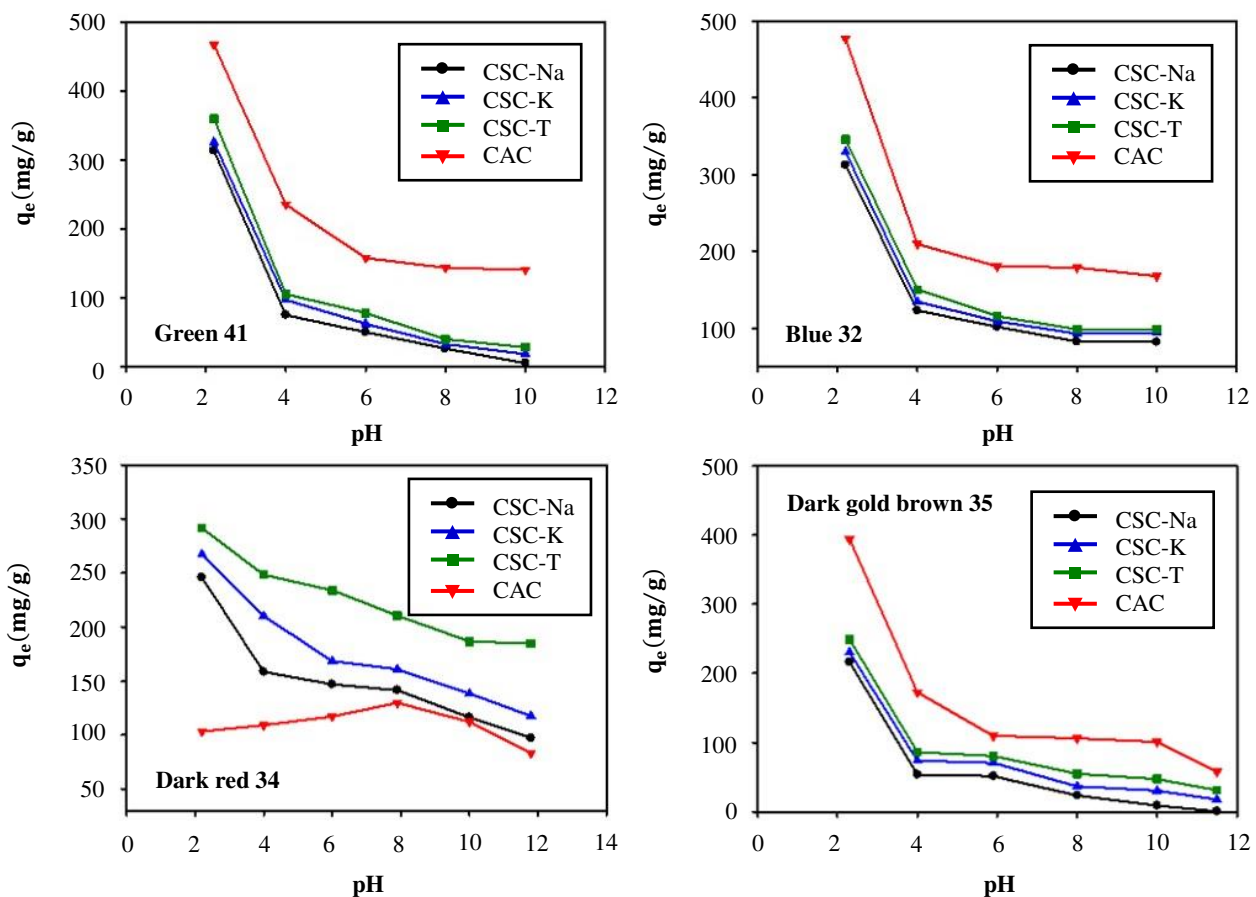

Figure 7 Effect of initial pH on adsorption of real silk dyes (C_o = 100 mg/L; amount of adsorbent 0.01 g/50 mL; room temperature)

3.5 Adsorption isotherm stud

The equilibrium data were analyzed by the most common isotherm models that are Langmuir and Freundlich models. The Langmuir model proposes monolayer coverage of adsorbate molecules onto a solid surface. Once the adsorbent site is covered with the dye molecules, no further adsorption occurs at that site [33]. The Langmuir model does not explain the adsorption mechanism but it provides information on adsorption capacity and the equilibrium process [33]. The Langmuir model in its nonlinear form is expressed as

$$q_e = \frac{q_m K_L C_e}{1 + K_L C_e} \tag{5}$$

where q_e is the adsorption capacity at equilibrium, q_m is the maximum adsorption capacity, C_e is the silk dye concentration in solution at equilibrium and K_L is the Langmuir constant related to the energy of adsorption. The graph is characterized by a plateau or an equilibrium saturation point where once a molecule occupies a site, no further adsorption can occur. The Freundlich model is based on the assumption that the adsorption occurs on a heterogeneous surface. It is applicable for both monolayer adsorption (chemisorption) and multilayer adsorption (Van der Waals adsorption) [33]. The nonlinear expression of the Freundlich equation is given as

$$q_e = K_F C_e^{1/n} \tag{6}$$

where K_F is the Freundlich constants and $1/n$ is the heterogeneity factor. The Freundlich equation is characterized by an adsorption isotherm lacking a plateau, indicated multilayer adsorption [33].

From Figure 8, the adsorption of silk dyes increased with an increase in initial dye concentration due to the higher driving force. Figure 8 also shows the plots of non-linear Langmuir and Freundlich isotherm models and the equilibrium parameters are listed in Table 6. The Langmuir isotherm model accurately described the adsorption process with high R^2 (> 0.98), indicating that the surfaces of all adsorbents were homogeneous and monolayer adsorption of silk dyes took place. It is important to note that the maximum adsorption capacities of silk dyes on the obtained carbon-silica composites were comparable to that of CAC.
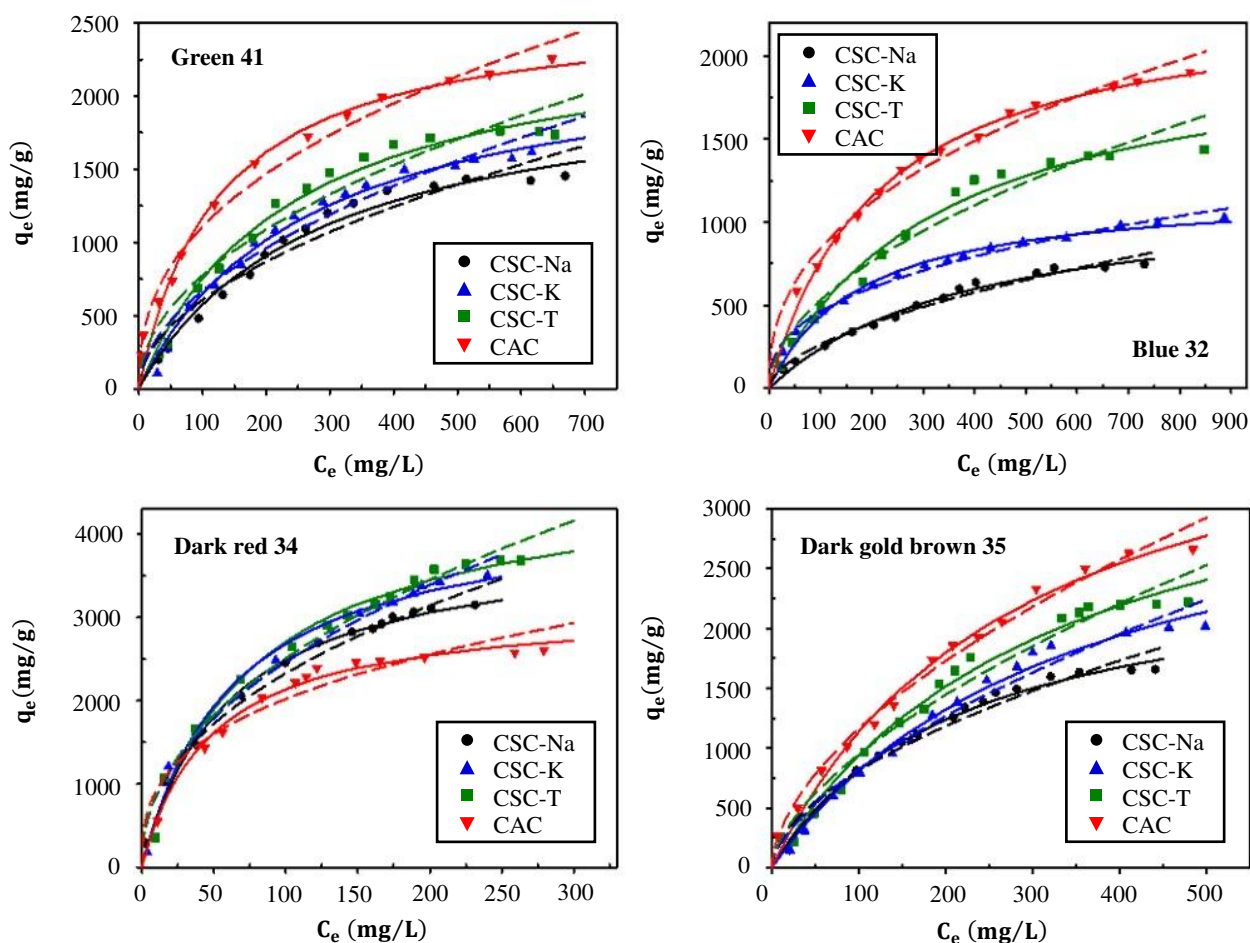

Figure 8 Equilibrium curves for real silk dyes adsorption with symbol = experimental data, solid line = Langmuir model, dashed line = Freundlich model (C_o = 50-1000 mg/L; amount of adsorbent 0.01 g/50 mL; room temperature)

Table 6 Equilibrium parameters for real silk dyes adsorption on the carbon-silica composites and commercial activated carbon

Isotherm models	Parameters	Adsorbent			
		CSC-Na	CSC-K	CSC-T	CAC
	Green 41				
Langmuir	q_m (mg/g)	2174.84	2361.03	2510.85	2625.10
	K_L (L/mg)	0.004	0.004	0.004	0.008
	R^2	0.980	0.988	0.981	0.984
Freundlich	K_F ((mg/g)(L/mg)$^{1/n}$)	55.99	59.14	81.12	169.98
	$1/n$	0.517	0.526	0.490	0.407
	R^2	0.930	0.944	0.923	0.946
	Blue 32				
Langmuir	q_m (mg/g)	1191.69	1198.20	2134.29	2374.46
	K_L (L/mg)	0.002	0.006	0.003	0.005
	R^2	0.989	0.983	0.983	0.992
Freundlich	K_F ((mg/g)(L/mg)$^{1/n}$)	19.96	77.41	46.70	128.50
	$1/n$	0.561	0.388	0.528	0.401
	R^2	0.973	0.976	0.948	0.978
	Dark red 34				
Langmuir	q_m (mg/g)	3974.47	4353.70	4735.17	3148.69
	K_L (L/mg)	0.017	0.016	0.013	0.021
	R^2	0.993	0.992	0.988	0.985
Freundlich	K_F ((mg/g)(L/mg)$^{1/n}$)	316.41	296.27	302.01	424.91
	$1/n$	0.433	0.460	0.460	0.338
	R^2	0.984	0.982	0.972	0.885

Table 6 (Continued) Equilibrium parameters for real silk dyes adsorption on the carbon-silica composites and commercial activated carbon

Isotherm models	Parameters	Adsorbent			
		CSC-Na	CSC-K	CSC-T	CAC
	Dark gold brown 35				
Langmuir	q_m (mg/g)	2580.29	3633.08	3941.95	4339.89
	K_L (L/mg)	0.005	0.003	0.003	0.004
	R^2	0.992	0.986	0.984	0.989
Freundlich	K_F ((mg/g)(L/mg)$^{1/n}$)	65.45	47.13	57.21	83.13
	$1/n$	0.546	0.621	0.610	0.573
	R^2	0.958	0.959	0.955	0.975

3.6 Effect of temperature on silk dye adsorption

The effect of temperature on adsorption of real silk dyes onto CSCs was investigated at 303, 313 and 323 K. The adsorption capacities of CSCs increased with increasing temperature (Figure 9), suggesting that the dye adsorption was endothermic. The higher adsorption capacities at higher temperatures can be explained by the increasing mobility of dye molecules with increasing temperature. Thermodynamics parameters for the adsorption were calculated using the equation:

$$\ln K = -\frac{\triangle H^o}{RT} + \frac{\triangle S^o}{R} \tag{7}$$

where K is the distribution coefficient of adsorbent and equal to q_e/C_e, ΔH^o and ΔS^o are the standard enthalpy and the standard entropy, respectively, T is the temperature in Kelvin and R is the ideal gas constant. The plot of $\ln K$ versus $1/T$ is linear with slope ΔH^o and intercept ΔS^o. The Gibbs free energy change (ΔG^o) indicating the spontaneity of the adsorption process was calculated from:

$$\triangle G^o = -RT \ln K \tag{8}$$

All thermodynamic parameters obtained are summarized in Table 7. The negative values of ΔG^o indicated that the adsorption process was spontaneous and the increase in magnitude with increasing temperature shows an increase in feasibility of adsorption at higher temperatures [34]. The positive values of ΔH^o confirmed the endothermic adsorption process and the positive value of ΔS^o suggested an increase in disorder of solid-liquid interface of CSCs during silk dye adsorption.
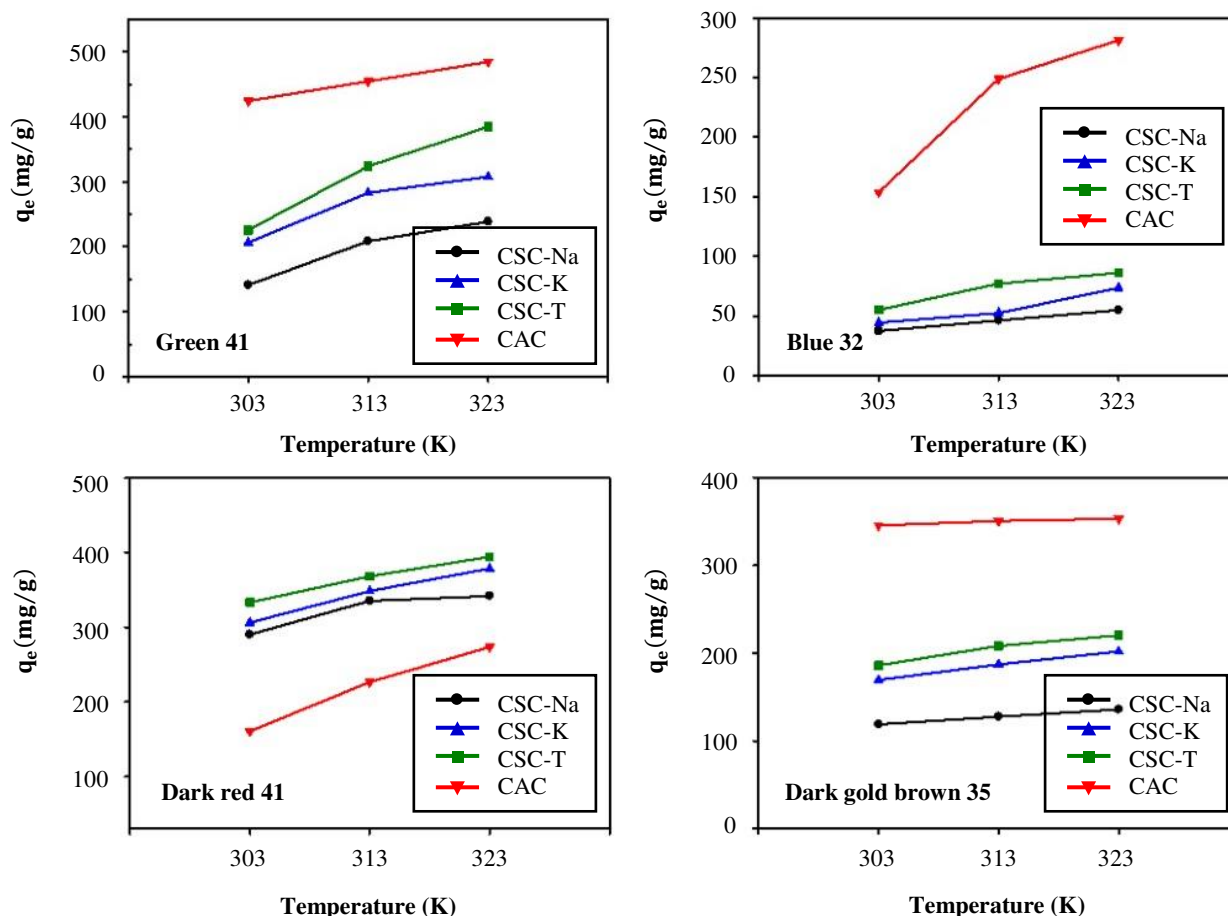

Figure 9 Effect of temperature on adsorption of real silk dyes (C_o = 100 mg/L; amount of adsorbent 0.01 g/50 mL)

Table 7 Thermodynamic properties of real silk dyes adsorbed on the carbon-silica composites and commercial activated carbon

Adsorbent	ΔG^o (kJ/mol)			ΔH^o (kJ/mol)	ΔS^o (kJ/mol·K)
	303 K	313 K	323 K		
Green 41					
CSC-Na	-15.66	-17.76	-19.00	35.09	0.17
CSC-K	-17.15	-19.37	-20.57	34.77	0.17
CSC-T	-17.97	-19.27	-20.04	13.60	0.10
CAC	-20.94	-21.81	-22.69	5.62	0.09
Blue 32					
CSC-Na	-8.32	-9.23	-10.06	18.16	0.09
CSC-K	-8.72	-9.62	-11.17	28.25	0.12
CSC-T	-9.46	-10.88	-11.63	23.48	0.11
CAC	-13.23	-17.18	-19.77	86.03	0.33
Dark red 34					
CSC-Na	-16.94	-18.52	-19.28	18.60	0.12
CSC-K	-17.28	-18.84	-20.29	28.30	0.15
CSC-T	-17.88	-18.81	-19.71	9.75	0.09
CAC	-14.21	-16.15	-17.60	37.09	0.17
Dark gold brown 35					
CSC-Na	-14.44	-15.20	-15.96	8.60	0.08
CSC-K	-15.95	-17.00	-17.99	15.01	0.10
CSC-T	-16.28	-17.30	-18.21	12.95	0.10
CAC	-25.80	-29.55	-30.94	52.40	0.26

4. Conclusions

Low-cost and effective carbon-silica composites for adsorption of silk dyes (Green 41, Dark gold brown 35, Blue 32 and Dark red 34) were prepared from vinasse with Na_2SiO_3 and K_2SiO_3 as low-cost silica sources. Under the optimum condition, the composites with maximum specific surface area of 375 and 343 m^2/g with mesopores structure could be produced from Na_2SiO_3 and K_2SiO_3, respectively. These composites had surface areas comparable to high cost and most commonly used silica source (TEOS, 656 m^2/g). The adsorption performance of the carbon-silica composites was evaluated with real silk dyes as adsorbates compared with a commercial activated carbon. The kinetics for silk dyes adsorption followed pseudo-second order model and the equilibrium data were well described by the Langmuir isotherm. It can be concluded that the moderate surface area mesoporous carbon-silica composites were superior to the microporous commercial activated carbon in view of the adsorption kinetics (faster adsorption) but had comparable adsorption capacities. To the best of our knowledge, this is the first study that prepared carbon-silica composites from vinasse and Na_2SiO_3 or K_2SiO_3. Consequently, these carbon-silica composites produced from industrial waste and low-cost silica sources could be used as adsorbents for various environmental application including dye removal from wastewater.

5. Acknowledgements

6. References

[1]   Vankar PS, Shukla D. Dyeing application of newer natural dyes on cotton silk and wool with fastness properties, CIE lab values, and shade card. In: Vankar PS, Shukla D, editors. New trends in natural dyes for textiles. Cambridge: Woodhead Publishing; 2019. p. 159-282.
[2]   Zonoozi MH, Moghaddam MRA, Arami M. Removal of acid red 398 dye from aqueous solutions by coagulation/flocculation process. Environ Eng Manag J. 2008;7(6):695-9.
[3]   Mook WT, Aroua MK, Szlachta M, Lee CS. Optimisation of reactive black 5 dye removal by electrocoagulation process using response surface methodology. Water Sci Technol. 2017;75(4):952-62.
[4]   Goswami M, Chaturvedi P, Kumar Sonwani R, Dutta Gupta A, Rani Singhania R, Shekher Giri B, et al. Application of Arjuna (*Terminalia arjuna*) seed biochar in hybrid treatment system for the bioremediation of Congo red dye. Bioresour Technol. 2020;307:123203.
[5]   Sterenzon E, Vadivel VK, Gerchman Y, Luxbacher T, Narayanan R, Mamane H. Effective removal of acid dye in synthetic and silk dyeing effluent: isotherm and kinetic studies. ACS Omega. 2022;7(1):118-28.
[6]   Reis CER, Bento HBS, Alves TM, Carvalho AKF, de Castro HF. Vinasse treatment within the sugarcane-ethanol industry using ozone combined with anaerobic and aerobic microbial processes. Environments. 2019;6(1):1-13.
[7]   Mao C, Zhang J, Xiao M, Liu Y, Zhang X. Carbon-silica composites supported Pt as catalyst for asymmetric hydrogenation of ethyl 2-oxo-4-phenylbutyrate. Curr Appl Phys. 2018;18(12):1480-5.
[8]   Sekunowo O, Durowaye S, Ogunsina O. Mechanical characterisation of carbon-silica reinforced composites for turbine application. J Inst Eng. 2019;15(1):166-9.
[9]   Chandran M, Shamna I, Anusha A, Bhagiyalakshmi M. Synthesis of mesoporous carbon-polymeric hybrid material for energy storage application. SN Appl Sci. 2019;1(6):1-10.
[10] Glover TG, Dunne KI, Davis RJ, LeVan MD. Carbon-silica composite adsorbent: characterization and adsorption of light gases. Microporous Mesoporous Mater. 2008;111(1-3):1-11.

[11] Gerasymenko N, Reyes RP, Espinosa MÁH, Mora ES, Petranovskii V. The adsorbing properties of mesoporous silica/carbon composites prepared by direct carbonization of the template as the sole source of the carbon phase. Adv Compos Lett. 2019;28:1-12.

[12] Cheong HS, Kang KK, Rhee HK. Preparation of titanium-containing carbon-silica composite catalysts and their liquid-phase epoxidation activity. Catal Lett. 2003;86(1-3):145-9.

[13] Twumasi E, Forslund M, Norberg P, Sjöström C. Carbon-silica composites prepared by the precipitation method. Effect of the synthesis parameters on textural characteristics and toluene dynamic adsorption. J Porous Mater. 2012;19:333-43.

[14] Fu L, Zhu J, Huang W, Fang J, Sun X, Wang X, et al. Preparation of nano-porous carbon-silica composites and its adsorption capacity to volatile organic compounds. Processes. 2020;8(3):372.

[15] Charmas B, Leboda R, Pikus S, Jezierski A, Kobylas E. Examination of the structure and energetic properties of carbosils surface prepared by dichloromethane pyrolysis. Colloids Surf A Physicochem Eng Asp. 2002;208(1-3):93-102.

[16] Sotiriou K, Supanchaiyamat N, Jiang T, Janekarn I, García AM, Budarin VL, et al. Synthesis and application of tuneable carbon-silica composites from the microwave pyrolysis of waste paper for selective recovery of gold from acidic solutions. RSC Adv. 2020;10(42):25228-38.

[17] Wiśniewska M, Wawrzkiewicz M, Onyszko M, Medykowska M, Nosal-Wiercińska A, Bogatyrov V. Carbon-silica composite as adsorbent for removal of hazardous C.I. basic yellow 2 and C.I. basic blue 3 dyes. Materials. 2021;14(12):3245.

[18] Noa-Bolaño A, Pérez-Ones O, Zumalacárregui-de Cárdenas L, Pérez-de los Ríos JL. Simulation of concentration and incineration as an alternative for vinasses' treatment. Rev Mex Ing Quim. 2020;19(3):1265-75.

[19] Jiang T, Budarin VL, Shuttleworth PS, Ellis G, Parlett CMA, Wilson K, et al. Green preparation of tuneable carbon-silica composite materials from wastes. J Mater Chem. 2015;3(27):14148-56.

[20] Valle-Vigón P, Sevilla M, Fuertes AB. Carboxyl-functionalized mesoporous silica-carbon composites as highly efficient adsorbents in liquid phase. Microporous Mesoporous Mater. 2013;176:78-85.

[21] Dakroury GA, Abo-Zahra SF, Hassan HS, Fathy NA. Utilization of silica-chitosan nanocomposite for removal of $^{152+154}$Eu radionuclide from aqueous solutions. J Radioanal Nucl Chem. 2020;323(1):439-55.

[22] Shweta K, Jha H. Rice husk extracted lignin-TEOS biocomposites: effects of acetylation and silane surface treatments for application in nickel removal. Biotechnol Rep. 2015;7:95-106.

[23] Wu T, Ke Q, Lu M, Pan P, Zhou Y, Gu Z, et al. Recent advances in carbon-silica composites: preparation, properties, and applications. Catalysts. 2022;12(5):573.

[24] Abate GY, Alene AN, Habte AT, Addis YA. Adsorptive removal of basic green dye from aqueous solution using humic acid modified magnetite nanoparticles: kinetics, equilibrium and thermodynamic studies. J Polym Environ. 2021;29(3):967-84.

[25] Geçgel Ü, Kocabıyık B, Üner O. Adsorptive removal of methylene blue from aqueous solution by the activated carbon obtained from the fruit of *Catalpa bignonioides*. Water Air Soil Pollut. 2015;226(8):1-14.

[26] Mahmoodi NM, Sadeghi U, Maleki A, Hayati B, Najafi F. Synthesis of cationic polymeric adsorbent and dye removal isotherm, kinetic and thermodynamic. J Ind Eng Chem. 2014;20(5):2745-53.

[27] Liu QX, Zhou YR, Wang M, Zhang Q, Ji T, Chen TY, et al. Adsorption of methylene blue from aqueous solution onto viscose-based activated carbon fiber felts: kinetics and equilibrium studies. Adsorp Sci Technol. 2019;37(3-4):312-32.

[28] Fathy N, El-Khouly S, Ahmed S, El-Nabarawy T, Tao Y. Superior adsorption of cationic dye on novel bentonite/carbon composites. Asia-Pac J Chem Eng. 2020;16(1):e2586.

[29] Balarak D, Mahdavi Y. Experimental and kinetic studies on acid red 88 dye (AR88) adsorption by *Azolla filiculoides*. Biochem Physiol. 2016;5:1-5.

[30] Su X, Liu L, Zhang Y, Liao Q, Yu Q, Meng R, et al. Efficient removal of cationic and anionic dyes from aqueous solution using cellulose-g-p(AA-co-AM) bio-adsorbent. Bioresources. 2017;12(2):3413-24.

[31] Balarak D, Pirdadeh F, Mahdavi Y. Biosorption of Acid Red 88 dyes using dried *Lemna minor* biomass. J Sci Technol Environ Inform. 2015;01(02):81-90.

[32] Alam MS, Khanom R, Rahman MA. Removal of Congo red dye from industrial wastewater by untreated sawdust. Am J Environ Prot. 2015;4(5):207-13.

[33] Jasper EE, Ajibola VO, Onwuka JC. Nonlinear regression analysis of the sorption of crystal violet and methylene blue from aqueous solutions onto an agro-waste derived activated carbon. Appl Water Sci. 2020;10:1-11.

[34] Boukhemkhem A, Rida K. Improvement adsorption capacity of methylene blue onto modified Tamazert kaolin. Adsorp Sci Technol. 2017;35(9-10):753-73.